Signal Processing 128 (2016) 531–545

Contents lists available at ScienceDirect

Signal Processing

journal homepage: www.elsevier.com/locate/sigpro

Inter-frame distortion drift analysis for reversible data hiding in encrypted H.264/AVC video bitstreams

Yuanzhi Yao, Weiming Zhang, Nenghai Yu*

Department of Electronic Engineering and Information Science, University of Science and Technology of China, Hefei 230027, China

ARTICLE INFO

Article history:
Received 12 December 2015
Received in revised form
1 May 2016
Accepted 2 May 2016
Available online 3 May 2016

Keywords:
Reversible data hiding
Video encryption
Inter-frame distortion drift
Coefficient selection
Histogram shifting

ABSTRACT

Due to the privacy-preserving requirement for cloud data management, it is necessary to perform data hiding in the encrypted domain. This paper proposes an effective scheme for reversible data hiding in encrypted H.264/AVC video bitstreams. In the encryption phase, the codewords of intra prediction modes, motion vector differences and partial residual coefficients are encrypted without video bit rate increment for preserving the confidentiality of video content. In the data hiding phase, we first present a theoretical analysis of the picture distortion caused by data embedding and the subsequent inter-frame distortion drift. Based on the analysis, we estimate the embedding distortions caused by modifying different residual coefficients and embed data into residual coefficients with different priorities for decreasing the inter-frame distortion drift. The data embedding is implemented by the histogram shifting technique. If the receiver decrypts the encrypted video bitstream and extracts the embedded data, the original video bitstream can be perfectly recovered. In addition, if the receiver decrypts the encrypted video bitstream without extracting the embedded data, the bitstream can still be decoded to obtain the reconstructed video with good quality.

1. Introduction

In recent years, the rapid development of cloud computing and network technology brings about novel storage ways for digital videos. More and more users prefer to store their compressed video data in cloud servers for saving local storage resources and distributing video data efficiently. Given that cloud services are vulnerable to malicious attacks and untrustworthy administrators, it is necessary to store video bitstreams in the encrypted domain for avoiding privacy leakage. However, it is difficult for cloud servers to manage encrypted video bitstreams. One feasible solution is to embed additional authentication data into the encrypted video bitstream for access control and media annotation. Therefore, the joint scheme for video encryption and video data hiding has attracted considerable research interest.

Differing from traditional text/binary data encryption [1], video encryption usually requires that the encryption scheme should have low computing complexity and the encrypted bitstream should be format-compliant. Therefore, it is not practical to encrypt video data completely with traditional ciphers due to high computational cost. Alternatively, we can selectively encrypt a fraction of video data to improve efficiency and keep format compliant. Since H.264/AVC is one of the most widely used video coding standards [2], some schemes have been proposed to encrypt H.264/AVC videos. The schemes proposed in [3,4] encrypt videos by scrambling the intra prediction modes (IPM) of intra-coded macroblocks. The encryption is performed by using bitwise XOR (exclusive-OR) operation on the IPMs. An improved scheme in [5] encrypts not only the intra prediction modes but also the motion vector differences (MVD). Another scheme in [6] encrypts the intra prediction modes, the motion vector differences and the residual coefficients. In addition, the scheme in [7] proposes to encrypt other coding parameters such as the sequence parameter set and the picture parameter set. In the view of perturbing macroblock prediction, the intra prediction modes, the motion vector differences and the residual coefficients are key coding parameters which need to be encrypted. By scrambling these coding parameters, the decoded reconstructed video will be severely distorted so that the confidentiality of video content can be preserved.

Reversible data hiding (RDH) is a technique which embeds secret messages into a cover in the reversible manner. Reversibility means that the original cover can be losslessly recovered after the embedded messages are extracted. Reversible data hiding can be utilized for media annotation and integrity authentication. Recently, some effective methods about reversible data hiding in encrypted images have been proposed [8–12]. These methods

* Corresponding author.
E-mail addresses: yaoyz@mail.ustc.edu.cn (Y. Yao), zhangwm@ustc.edu.cn (W. Zhang), ynh@ustc.edu.cn (N. Yu).

http://dx.doi.org/10.1016/j.sigpro.2016.05.004
0165-1684/© 2016 Elsevier B.V. All rights reserved.

cannot be applied to reversible data hiding in encrypted videos directly. The major problem for video data hiding is how to decrease the distortion drift caused by data embedding, while this problem does not need to be discussed in reversible image data hiding. The distortion drift can severely degrade the reconstructed video quality. There exist two types of distortion drifts in video data hiding, which are the intra-frame distortion drift and the inter-frame distortion drift. To avert the intra-frame distortion drift, Ma et al. [13] proposed to use pairs of quantized DCT coefficients for data embedding so that the distortion in current cover block will not propagate to its neighboring blocks. A compensation method proposed in [14] eliminates the intra-frame distortion drift by obtaining the difference between the original and modified reconstructed quantized DCT coefficients and compensating for the quantized DCT coefficients. Two reversible video data hiding methods which discuss data embedding in inter-coded frames can be found in [15,16]. Gujjunoori et al. [15] proposed to embed two bits into the zero quantized DCT coefficients in the fixed position. Bouchama et al. [16] brought modifications to Gujjunoori et al.'s method [15] for improving the embedding capacity and the video quality. Bouchama et al.'s method [16] can embed three bits into a set of quantized DCT coefficients according to the predefined mapping rule. However, these methods [15,16] do not consider decreasing the inter-frame distortion drift. To the best of our knowledge, almost no encrypted video data hiding method focuses on decreasing the inter-frame distortion drift in the open literature. Besides, the inter-frame distortion drift is more influential than the intra-frame distortion drift because the inter prediction is usually more frequently used than the intra prediction in video coding. Therefore, how to decrease the inter-frame distortion drift is a key and unresolved problem in encrypted video data hiding.

Because functionalities of video encryption and video data hiding are different, the joint scheme for video encryption and video data hiding should combine these two functionalities together to protect the confidentiality and authenticate the identification. Therefore, the joint scheme should support data embedding/extraction operation in the encrypted domain and keep the video bitstream format-compliant. For example, data can be embedded into the encrypted video bitstream without knowing the encryption key, or data can be extracted from the encrypted video bitstream without complete video decoding process. Lian et al. [17] proposed to encrypt the intra prediction modes, the signs of motion vector differences and the signs of DCT coefficients using stream ciphers and embed data in DCT coefficients. The quantization embedding is used in this scheme so that data embedding cannot be performed directly on the quantized DCT coefficients. In the scheme proposed by Park et al. [18], the intra prediction modes, the signs of motion vector differences and the signs of DCT coefficients are encrypted and data are embedded in intra prediction modes. However, the stego video bitstream is not fully format-compliant. Recently, Xu et al. [19] presented the scheme for data hiding in encrypted H.264/AVC video bitstreams by analyzing the codewords of context-adaptive variable length coding (CAVLC). In this scheme, video encryption and data embedding are performed using the codeword substitution technique. The major advantage of this scheme is that the video bitstream size is strictly preserved even after video encryption and data embedding.

Although the schemes [17–19] achieve video encryption and video data hiding together, their common drawback is that reversible data hiding is not applied. If the receiver decrypts the encrypted video and extracts the embedded data, he/she can only obtain the reconstructed video with degraded quality. Xu et al. proposed a scheme for reversible data hiding in the encrypted video bitstream [20] using the histogram shifting technique [21]. Differing from the encryption scheme in [19], the scheme in [20] encrypts the signs of all non-zero quantized DCT coefficients. However, if the sign of one non-zero quantized DCT coefficient is encrypted and its original *suffixLength*[1] is 0, its codeword structure may change. Therefore, the scheme in [20] may cause the video bit rate increment during the encryption process. Moreover, in some application scenarios, the receiver may download the video from the cloud server and view the decrypted reconstructed video using the encryption key. The decrypted video still contains the embedded authentication data, which is convenient for the cloud server to manage the video. At this time, the distortion drift caused by data embedding will degrade the reconstructed video quality. The scheme in [20] does not explore this problem like other existing schemes [15,16]. Hence, new reversible video data hiding schemes which are capable of decreasing the inter-frame distortion drift should be sought.

We propose an effective scheme for reversible data hiding in encrypted H.264/AVC video bitstreams in this paper. We mainly concentrate on decreasing the inter-frame distortion drift caused by data embedding. In the encryption phase, three types of key coding parameters including the intra prediction modes, the motion vector differences and the quantized DCT coefficients are selectively encrypted using stream ciphers without video bit rate increment. In the data hiding phase, to explore the fundamental principle of the video quality degradation caused by data embedding, we present a theoretical analysis of the inter-frame distortion drift, which is the central element of our proposed scheme. Based on the analysis, we estimate the embedding distortions caused by modifying different residual coefficients and embed data into residual coefficients with different priorities for decreasing the inter-frame distortion drift. The data embedding is implemented by the histogram shifting technique. In conclusion, the highlights of this paper can be summarized as follows.

- Video encryption can keep the bitstream format-compliant and the video bit rate constant.
- A theoretical analysis of the inter-frame distortion drift is presented.
- The proposed scheme can embed data in the video bitstream with low distortion based on the inter-frame distortion drift analysis.
- The video bitstream can be losslessly recovered after video decryption and data extraction.

The rest of the paper is organized as follows. In Section 2, we present the scheme for reversible data hiding in encrypted H.264/AVC video bitstreams. The experimental results are shown in Section 3. Finally, Section 4 concludes the paper.

2. Proposed scheme for reversible data hiding in encrypted H.264/AVC video bitstreams

In this section, the scheme for reversible data hiding in encrypted H.264/AVC video bitstreams is elaborated. The framework of the proposed scheme is shown in Fig. 1. The scheme is composed of three components: video encryption, data embedding in encrypted video, and data extraction and video recovery. In the encryption phase, the content owner encrypts the original H.264/AVC video bitstream using stream ciphers to obtain the encrypted video bitstream. In the data hiding phase, the data hider (e.g., a database manager or a cloud server) can embed some additional authentication data into the encrypted video bitstream without

[1] The *suffixLength* is a syntax element for encoding the suffix length of the codeword of *Level*.

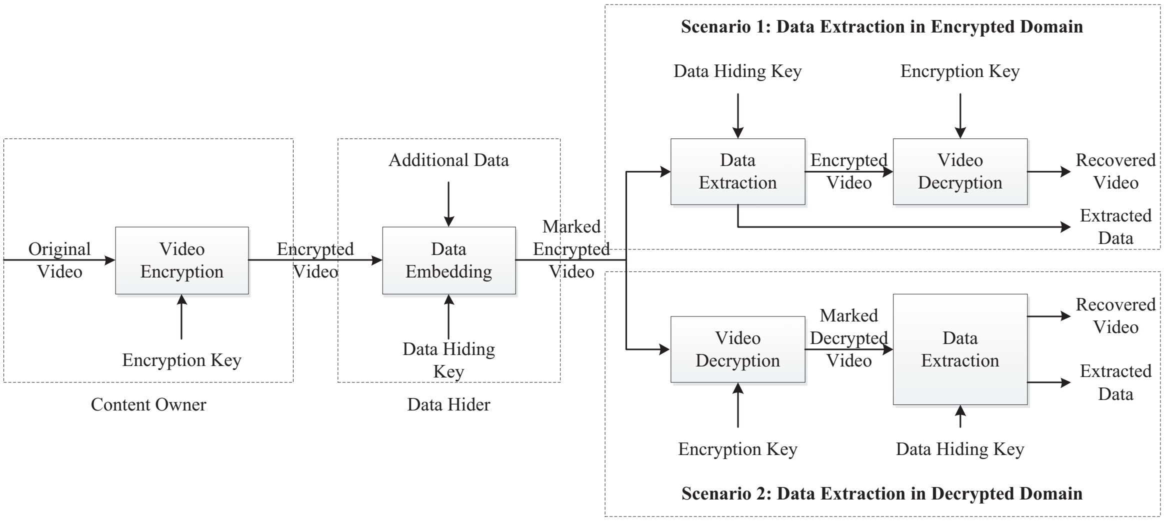

Fig. 1. Framework of the proposed scheme for reversible data hiding in encrypted H.264/AVC video bitstreams.

knowing the content of original video. At the receiver end, the content owner himself or an authorized third party can extract the embedded data either in the encrypted domain or in the decrypted domain. If the receiver decrypts the encrypted video bitstream and extracts the embedded data, the original video bitstream can be perfectly recovered, as depicted in Scenario 1 in Fig. 1. In addition, if the receiver decrypts the encrypted video bitstream without extracting the embedded data, the bitstream can still be decoded to obtain the reconstructed video with good quality, as depicted in Scenario 2 in Fig. 1.

2.1. H.264/AVC video encryption

Selective encryption is one of the most practical techniques for video data. Because it can decrease computing complexity and have adequate perceptual scrambling effect by encrypting some key coding parameters. Besides, selective encryption can keep the bitstream format-compliant to allow the video decoder to identify bitstream structure without decryption. In [20], it is suggested that the intra prediction modes (IPM), the signs of motion vector differences and the signs of quantized DCT coefficients are encrypted using the standard stream cipher RC4. However, as pointed out in [22], cryptographic algorithms get weaker over time, including RC4. Therefore, to encrypt these coding parameters, we use the novel stream cipher Spritz [22] in the proposed scheme. Spritz attempts to remedy the weakness in RC4 and remain its general design principles. Differing from [20], the signs of quantized DCT coefficients are selectively encrypted to keep video bit rate constant after encryption.

2.1.1. Intra prediction mode (IPM) encryption

In H.264/AVC, four types of intra prediction modes are supported, including Intra_4 × 4, Intra_16 × 16, Intra_chroma and I_PCM [2]. Because Intra_4 × 4 and Intra_16 × 16 are frequently used in intra prediction coding, we selectively encrypt these two modes to scramble the intra prediction of blocks. When utilizing the Intra_16 × 16 mode, the whole luma component of a macroblock is predicted. There are four different prediction modes for an Intra_16 × 16 block [23]. The last bit of each codeword for Intra_16 × 16 mode is encrypted by applying the bitwise XOR operation with a pseudo-random bit to keep the codeword length constant [4]. Pseudo-random bits are generated by an encryption key *E_Key*1 using the stream cipher Spritz. When utilizing the Intra_4 × 4 mode, each 4 × 4 block is predicted from its spatially neighboring samples. There are nine different prediction modes for an Intra_4 × 4 block, ranging from mode 0 to mode 8 [23]. The predictive coding technique is applied for efficiently compressing the prediction mode. If the prediction mode *Mode* of the currently considered block is equal to the most probable mode *MPM*, the codeword for Intra_4 × 4 mode should keep unchanged. Otherwise, three bits of fixed-length code in each codeword for Intra_4 × 4 mode are encrypted by applying the bitwise XOR operation with a pseudo-random sequence [6]. The pseudo-random sequence is generated by an encryption key *E_Key*2 using the stream cipher Spritz. According to H.264/AVC standard [23], the length of the encrypted codeword for intra prediction mode can be the same as the original one.

2.1.2. Motion vector difference (MVD) encryption

In order to scramble the inter prediction of blocks, the motion vectors should also be encrypted. To improve the compression efficiency, motion vector prediction is further performed on the motion vector to obtain the motion vector difference (MVD). In H.264/AVC baseline profile, Exp-Golomb entropy coding is used to encode MVDs [23]. The structure of Exp-Golomb codeword is $[Mzeros][1][INFO]$, in which $[Mzeros]$ are M leading bits and $[INFO]$ is an M-bit data carrying information. The codeword length is $(2M + 1)$. The last bit of each codeword is encrypted by applying the bitwise XOR operation with a pseudo-random bit. Pseudo-random bits are generated by an encryption key *E_Key*3 using the stream cipher Spritz. When the value of MVD is equal to 0, its corresponding codeword "1" should keep unchanged during the encryption process. Encrypting the last bit of each codeword may change the sign of MVD, but does not affect the codeword length [17].

2.1.3. Residual coefficient encryption

To further protect the confidentiality of video content, the residual coefficients of each frame should also be encrypted. In H.264/AVC baseline profile, the context-adaptive variable length coding (CAVLC) is used to encode the quantized DCT coefficients of each residual block [23]. To decrease computing complexity and keep format compliant, not all syntax elements need to be encrypted. Therefore, the signs of quantized DCT coefficients are scrambled by encrypting corresponding codewords of *trailing_ones_sign_flag* and *Level*.

The one-bit codeword of *trailing_ones_sign_flag* is encrypted by applying the bitwise XOR operation using the stream cipher Spritz, which is determined by an encryption key *E_Key*4. The codeword of each *Level* is made up of a prefix level_*prefix* and a suffix

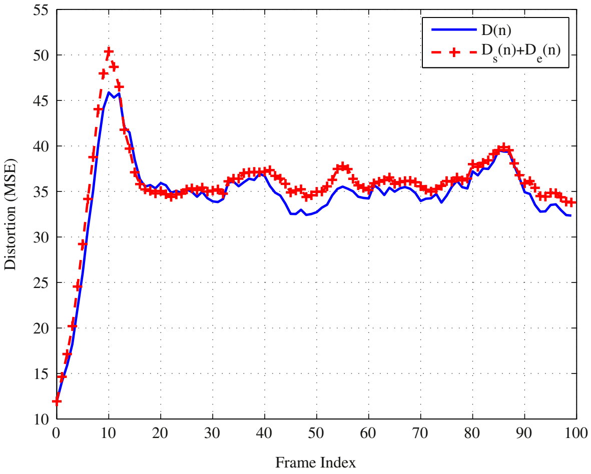

Fig. 2. Comparison between $D(n)$ and $D_s(n)+D_e(n)$ for QCIF video sequence Foreman at embedding rate 10% using QP 28.

level_suffix as [*level_prefix*][*level_suffix*]. The last bit of each codeword is encrypted by applying the bitwise XOR operation with a pseudo-random bit. Pseudo-random bits are generated by an encryption key *E_Key*5 using the stream cipher Spritz. It should be noted that when *suffixLength* is equal to 0, the corresponding codeword of *Level* should not be encrypted to keep the codeword length constant [19].

2.2. Data embedding in encrypted video

The data hider can embed some additional authentication data into the encrypted video bitstream without knowing the content of original video for access control and media annotation. Reversible data hiding can be used to recover the video bitstream losslessly after video decryption and data extraction. When the receiver views the decrypted reconstructed video without extracting the embedded data, the distortion drift caused by data embedding will degrade the reconstructed video quality. Therefore, we should endeavor to decrease the inter-frame distortion drift caused by data embedding.

2.2.1. Inter-frame distortion drift analysis

We first present a theoretical analysis of the picture distortion caused by data embedding and the subsequent inter-frame distortion drift. The theoretical analysis is inspired by the source and channel rate-distortion analysis in [24]. To analyze the inter-frame distortion drift and its influence on the visual quality of the reconstructed video, we consider the video in the decrypted domain.[2] Besides, we only focus on the distortion drift of P-frames, because B-frames do not cause distortion drift. Let $F(n,i)$ be the original luma value of pixel i in the nth video frame and $\hat{F}(n,i)$ be the corresponding reconstructed luma value of pixel i in the feedback loop at the encoder. We denote the reconstructed luma value of pixel i at the receiver end as $\tilde{F}(n,i)$. $\tilde{F}(n,i)$ may be different from $\hat{F}(n,i)$ due to data embedding. For inter-coded macroblocks, let $r(n,i)$ be the motion compensation residue at the encoder. Let $\tilde{r}(n,i)$ and $\hat{r}(n,i)$ be the corresponding reconstructed values with embedded data and without embedded data respectively. Because the positions and the number of embedded message bits can be random, $\tilde{F}(n,i)$ and $\hat{F}(n,i)$ are actually random variables. Therefore, we can model and analyze the overall distortion $D(n)$ of the nth video frame at the receiver end which is given by

$$D(n) = \mathrm{E}\{[\tilde{F}(n,i) - F(n,i)]^2\} \tag{1}$$

$\mathrm{E}\{x(n,i)\}$ is denoted as the average (over all pixels) expected value of the random variable $x(n,i)$. The source distortion $D_s(n)$ caused by lossy compression and the embedding distortion $D_e(n)$ caused by embedding data in quantized DCT coefficients of the nth video frame are respectively given by

$$D_s(n) = \mathrm{E}\{[\hat{F}(n,i) - F(n,i)]^2\} \tag{2}$$

$$D_e(n) = \mathrm{E}\{[\tilde{F}(n,i) - \hat{F}(n,i)]^2\} \tag{3}$$

In this paper, we assume that $D_s(n)$ and $D_e(n)$ are uncorrelated with each other. That is to say

$$D(n) = D_s(n) + D_e(n) \tag{4}$$

To justify this assumption, we encode four QCIF video sequences[3] [25] which are Carphone, Foreman, Hall and Salesman at frame rate 30 fps with the H.264/AVC reference software JM 10.2 [26]. The GOP (Group of Picture) structure is IPPP. The data embedding starts in the first P-frame in the GOP and then proceeds to subsequent P-frames. We use the histogram shifting technique proposed in [21] to embed message bits in the quantized luma DCT coefficients of each P-frame. We denote T_p and T_n as the two highest bins in the histogram of quantized DCT coefficients. (Zero coefficients are not used for data embedding.) Bellifemine et al. [27] had pointed out that the 2D DCT coefficients of the differential signal tend to be less correlated if the motion estimation is used. Thus, the distribution of DCT coefficients can be well modeled with the Laplacian probability distribution [28]. This proposition reveals that T_p=1 and $T_n = -1$ respectively. When we choose bin T_p and bin T_n as the actual data embedding zone, the embedding capacity is the sum of the number of bin T_p and the number of bin T_n. The embedding rate γ can be defined as the ratio of the number of actual embedded message bits m to the embedding capacity. In Fig. 2, we plot $D(n)$ and $D_s(n)+D_e(n)$ for each frame of QCIF video sequence Foreman at embedding rate 10% using QP 28. It can be seen that $D(n)$ is approximately equal to $D_s(n)+D_e(n)$. The average relative difference e_D between $D(n)$ and $D_s(n)+D_e(n)$ is defined by

$$e_D = \frac{1}{N}\sum_{n=1}^{N}\frac{|[D_s(n)+D_e(n)] - D(n)|}{D(n)} \times 100\% \tag{5}$$

where N is the total number of video frames. We perform similar tests on other video sequences and embedding rates. The average relative difference for each test is listed in Table 1. It can be seen that e_D is very small. This implies that it is quite reasonable to assume that the source distortion $D_s(n)$ and the embedding distortion $D_e(n)$ are uncorrelated with each other and that $D(n) = D_s(n) + D_e(n)$. Given the original video bitstream, $D_s(n)$ is constant. Therefore, to decrease the overall distortion $D(n)$ and improve the decoded reconstructed video quality, the only thing left is to estimate $D_e(n)$ and endeavor to decrease it during data embedding.

We suppose that the GOP structure is IPPP, in which only the first frame is encoded as an I-frame and the remaining frames are encoded as P-frames. For a pixel in the inter-coded macroblock of the nth frame ($n \geq 2$) at the receiver end, in case of no embedded data, its reconstructed value is $\tilde{F}(n-1,j) + \hat{r}(n,i)$ where pixel j is

[2] We analyze the inter-frame distortion drift in the decrypted domain because the receiver may view the decrypted reconstructed video without extracting the embedded data. In this scenario, how to decrease the inter-frame distortion drift is key to improve the reconstructed video quality.

[3] The video sequence can be a series of raw images or a series of decompressed images obtaining from the video bitstream.

Table 1
Average relative difference e_D between $D(n)$ and $D_s(n)+D_e(n)$.

Video sequence	Quantization parameter	Embedding rate (%)	Average relative difference e_D (%)
Carphone	28	10	0.0240
Carphone	24	20	0.0491
Foreman	28	10	0.0319
Foreman	24	20	0.0505
Hall	28	10	0.0224
Hall	24	20	0.0016
Salesman	28	10	0.0326
Salesman	24	20	0.0253

the motion prediction of pixel i. (If the sub-pixel motion estimation is used, j could point to a sub-pixel position.) If the macroblock contains embedded data, its reconstructed value is $\tilde{F}(n-1,j)+\tilde{r}(n,i)$. Therefore, the expected embedding distortion is

$$\begin{aligned}
D_e(n) &= \mathrm{E}\{[\tilde{F}(n,i)-\hat{F}(n,i)]^2\}\\
&= (1-p)\cdot\mathrm{E}\{[\tilde{F}(n-1,j)+\hat{r}(n,i)-\hat{F}(n,i)]^2\}\\
&\qquad + p\cdot\mathrm{E}\{[\tilde{F}(n-1,j)+\tilde{r}(n,i)-\hat{F}(n,i)]^2\}\\
&= (1-p)\cdot\mathrm{E}\{[\tilde{F}(n-1,j)-\hat{F}(n-1,j)]^2\}\\
&\qquad + p\cdot\mathrm{E}\{[\tilde{F}(n-1,j)+\tilde{r}(n,i)-\hat{F}(n-1,j)-\hat{r}(n,i)]^2\}\\
&= (1-p)\cdot\mathrm{E}\{[\tilde{F}(n-1,j)-\hat{F}(n-1,j)]^2\}\\
&\qquad + p\cdot\mathrm{E}\{[\tilde{F}(n-1,j)-\hat{F}(n-1,j)]^2\} + p\cdot\mathrm{E}\{[\tilde{r}(n,i)-\hat{r}(n,i)]^2\}\\
&\qquad + 2p\cdot\mathrm{E}\{[\tilde{F}(n-1,j)-\hat{F}(n-1,j)][\tilde{r}(n,i)-\hat{r}(n,i)]\}\\
&= (1-p)\cdot\mathrm{E}\{[\tilde{F}(n-1,j)-\hat{F}(n-1,j)]^2\}\\
&\qquad + p\cdot\mathrm{E}\{[\tilde{F}(n-1,j)-\hat{F}(n-1,j)]^2\} + p\cdot\mathrm{E}\{[\tilde{r}(n,i)-\hat{r}(n,i)]^2\} \quad (6)
\end{aligned}$$

where p is the probability of embedding data in the nth frame. It should be noted that the fifth identity in Eq. (6) is based on the assumption that $\mathrm{E}\{[\tilde{F}(n-1,j)-\hat{F}(n-1,j)][\tilde{r}(n,i)-\hat{r}(n,i)]\}=0$. The proof of the assumption in Eq. (6) is presented in Appendix A. If we assume that

$$\mathrm{E}\{[\tilde{F}(n-1,j)-\hat{F}(n-1,j)]^2\}=\alpha\cdot D_e(n-1) \quad (7)$$

where α is a constant relating to the video content, we can rewrite Eq. (6) as

$$\begin{aligned}
D_e(n) &= [(1-p)\alpha+p\alpha]\cdot D_e(n-1)+p\cdot\mathrm{E}\{[\tilde{r}(n,i)-\hat{r}(n,i)]^2\}\\
&= \alpha\cdot D_e(n-1)+p\cdot\mathrm{E}\{[\tilde{r}(n,i)-\hat{r}(n,i)]^2\} \quad (8)
\end{aligned}$$

It can be seen from Eq. (8) that the embedding distortion $D_e(n)$ of the nth frame is the sum of $\alpha\cdot D_e(n-1)$ and $p\cdot\mathrm{E}\{[\tilde{r}(n,i)-\hat{r}(n,i)]^2\}$. We can obtain two propositions from Eq. (8). One proposition is that we should endeavor to decrease $\mathrm{E}\{[\tilde{r}(n,i)-\hat{r}(n,i)]^2\}$ for decreasing the embedding distortion in the nth frame. Another proposition is that the embedding distortion of each frame can accumulate as the frame index increases. This is defined as the inter-frame distortion drift.

2.2.2. *Inter-frame distortion drift prevention*

Based on the inter-frame distortion drift analysis, we investigate the discrete cosine transform in H.264/AVC standard for decreasing the inter-frame distortion drift. In H.264/AVC, integer 4 × 4 transform can be computed exactly in arithmetic and can avoid mismatch problem in inverse transform [23]. The 4 × 4 transform is depicted in Eq. (9).

$$Y=C_f R C_f^T \quad (9)$$

where

$$C_f=\begin{pmatrix}1 & 1 & 1 & 1\\ 2 & 1 & -1 & -2\\ 1 & -1 & -1 & 1\\ 1 & -2 & 2 & -1\end{pmatrix}$$

In Eq. (9), Y is the matrix of original unscaled luma DCT coefficients corresponding to the residual 4 × 4 block R. Then, the post-scaling and quantization step is given in Eq. (10).

$$Z=\mathrm{round}[Y.\times PF./Qstep] \quad (10)$$

where $.\times$ and $./$ are denoted as the element-wise product operator of matrices and the element-wise division operator of matrices respectively. In Eq. (10), $Z=(z_{ij})_{4\times4}$ is the quantized DCT coefficient matrix in the 4 × 4 block and $Qstep$ is the quantization step size which is determined by QP. (QP is the quantization parameter.) PF is the quantization matrix which is given by

$$PF=\begin{pmatrix}a^2 & ab/2 & a^2 & ab/2\\ ab/2 & b^2/4 & ab/2 & b^2/4\\ a^2 & ab/2 & a^2 & ab/2\\ ab/2 & b^2/4 & ab/2 & b^2/4\end{pmatrix} \quad a=\frac{1}{2} \quad b=\sqrt{\frac{2}{5}}$$

Then, the quantized DCT coefficients will undergo the entropy encoding.

At the feedback loop at the encoder, after inverse quantization step in Eq. (11), the reconstructed residual block $\hat{R}=(\hat{r}_{ij})_{4\times4}$ without embedded data can be obtained in Eq. (12).

$$\hat{Y}=Z.\times Qstep.\times PF.\times 64 \quad (11)$$

$$\hat{R}=\mathrm{round}[(C_i^T\hat{Y}C_i)./64]=\mathrm{round}[C_i^T(Z.\times Qstep.\times PF)C_i] \quad (12)$$

where

$$C_i=\begin{pmatrix}1 & 1 & 1 & 1\\ 1 & 1/2 & -1/2 & -1\\ 1 & -1 & -1 & 1\\ 1/2 & -1 & 1 & -1/2\end{pmatrix}$$

After data embedding, the message bits are embedded in the quantized DCT coefficients as depicted in Eq. (13), where $\triangle=(\delta_{ij})_{4\times4}$ is the error matrix added to the quantized DCT coefficient matrix Z in the 4 × 4 block as follows.

$$Z'=Z+\triangle \quad (13)$$

After inverse quantization step in Eq. (14), the reconstructed residual block $\tilde{R}=(\tilde{r}_{ij})_{4\times4}$ with embedded data can be obtained in Eq. (15).

$$\begin{aligned}
\tilde{Y} &= Z'.\times Qstep.\times PF.\times 64\\
&= Z.\times Qstep.\times PF.\times 64+\triangle.\times Qstep.\times PF.\times 64 \quad (14)
\end{aligned}$$

$$\begin{aligned}
\tilde{R} &= \mathrm{round}[(C_i^T\tilde{Y}C_i)./64]\\
&= \mathrm{round}[C_i^T(Z.\times Qstep.\times PF)C_i+C_i^T(\triangle.\times Qstep.\times PF)C_i] \quad (15)
\end{aligned}$$

The error matrix E of the pixel luma value between the reconstructed residual block $\tilde{R}$ with embedded data and the reconstructed residual block $\hat{R}$ without embedded data can be calculated as depicted in Eq. (16), where $E=(e_{ij})_{4\times4}$.

$$\begin{aligned} E &= \tilde{R} - \hat{R} \\ &= \mathrm{round}[C_i^T(Z.\times Qstep.\times PF)C_i + C_i^T(\triangle.\times Qstep.\times PF)C_i] \\ &\quad - \mathrm{round}[C_i^T(Z.\times Qstep.\times PF)C_i] \end{aligned} \tag{16}$$

Let $z'_{ij}Z_{\sim i,j}$ be the matrix of quantized DCT coefficients in the 4×4 block obtained from the matrix Z whose δ_{ij} has been added into the (i,j)th coefficient z_{ij}. Without considering the rounding operator on coefficients, we can estimate[4] the independent embedding distortion $\rho_{ij}(Z, z'_{ij}Z_{\sim i,j})$ caused by modifying the (i,j)th coefficient in the 4×4 block using the MSE (Mean Squared Error) measure in Eq. (17).

$$\rho_{ij}(Z, z'_{ij}Z_{\sim i,j}) = \frac{1}{4\times4}\sum_{i=1}^{4}\sum_{j=1}^{4}(\tilde{r}_{ij}-\hat{r}_{ij})^2 = \begin{cases} \frac{25}{1024}Qstep^2b^4\delta_{ij}^2 & \text{if } (i,j)\in C_1 \\ \frac{5}{32}Qstep^2a^2b^2\delta_{ij}^2 & \text{if } (i,j)\in C_2 \\ Qstep^2a^4\delta_{ij}^2 & \text{if } (i,j)\in C_3 \end{cases} \tag{17}$$

where

$$\begin{cases} C_1 = \{(2,2),(4,2),(2,4),(4,4)\} \\ C_2 = \{(1,2),(2,1),(1,4),(2,3),(3,2),(4,1),(3,4),(4,3)\} \\ C_3 = \{(1,1),(3,1),(1,3),(3,3)\} \end{cases}$$

It can be known that $\frac{25}{1024}Qstep^2b^4\delta_{ij}^2 < \frac{5}{32}Qstep^2a^2b^2\delta_{ij}^2 < Qstep^2a^4\delta_{ij}^2$ by sorting independent embedding distortions. Therefore, we can classify coefficients based on their corresponding independent embedding distortions. In Eq. (17), C_1, C_2 and C_3 represent the coefficient classification sets. According to the linear property of 4×4 transform, it is easy to verify that the embedding distortion $D_e(\tilde{R},\hat{R})$ in the 4×4 block can be captured by the sum of the independent embedding distortion $\rho_{ij}(Z, z'_{ij}Z_{\sim i,j})$ in the form

$$D_e(\tilde{R},\hat{R}) = \mathrm{E}\{(\tilde{r}_{ij}-\hat{r}_{ij})^2\} = \sum_{i=1}^{4}\sum_{j=1}^{4}\rho_{ij}(Z, z'_{ij}Z_{\sim i,j}) \tag{18}$$

From Eqs. (17) and (18) we can infer that it is necessary to embed data using coefficient selection, which means that data should be embedded into the coefficients in C_1 with highest priority, the coefficients in C_2 with medium priority and the coefficients in C_3 with lowest priority. The coefficient classification illustration in the 4×4 block is given in Fig. 3. The coefficient selection aims to decrease the embedding distortion in the current frame.

To justify the proposition, we encode QCIF video sequence Foreman [25] at frame rate 30 fps using QP 28 with the H.264/AVC reference software JM 10.2 [26]. The first 100 frames are encoded and the GOP structure is IPPP. The data embedding starts in the first P-frame in the GOP and then proceeds to subsequent P-frames. We use the histogram shifting technique proposed in [21] to embed message bits in the quantized luma DCT coefficients of each P-frame. We choose bin $T_p=1$ and bin $T_n=-1$ as the actual data embedding zone. In the data embedding zone, the numbers of coefficients belonging to C_1, C_2 and C_3 are 2810, 12,230 and 14,646 respectively. (If a macroblock in the P-frame is intra-coded or its coding mode is P_Skip, it is not used for data embedding.) We embed 2000 message bits in coefficients belonging to C_1, C_2 and C_3 respectively to generate three stego videos[5] and plot their overall distortions in Fig. 4. It can be seen that embedding data into coefficients in C_1 can introduce the minimum distortion.

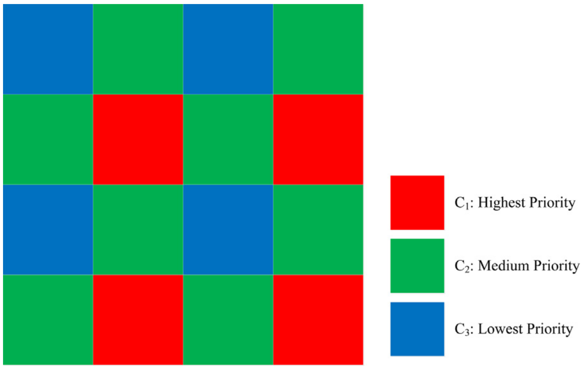

Fig. 3. Coefficient classification illustration in the 4×4 block.

Based on the inter-frame distortion drift analysis in Eq. (8), we design the inter-frame distortion drift prevention scheme for data embedding. Firstly, coefficient selection should be used in order to decrease the embedding distortion in each P-frame. Secondly, data embedding should start in the last frame in each GOP and then proceed to previous frames in order to decrease the embedding distortion accumulation.

2.2.3. *Data embedding*

Once the data hider acquires the encrypted video, he/she can embed some data into it without getting access to the original video. The histogram shifting technique [21] is used to embed data in the quantized luma DCT coefficients of each P-frame. Because the video encryption scheme only changes the signs of quantized DCT coefficients, the distribution of coefficients can still be modeled as the Laplacian probability distribution [28]. Therefore, we choose $T_p=1$ and $T_n=-1$ as the actual data embedding zone, where T_p and T_n are the two highest bins in the coefficient histogram. (Zero coefficients are not used for data embedding.) The embedding capacity C is the sum of the number of bin T_p and the number of bin T_n as depicted in Eq. (19).

$$C = \mathrm{num}(T_p) + \mathrm{num}(T_n) \tag{19}$$

During data embedding process, the proposed inter-frame distortion drift prevention scheme should be used. We suppose that the total frame number of the video is N and only the first frame is encoded as an I-frame. The GOP number is 1 and its structure is IPPP. We denote the to-be-embedded data as a binary message sequence $\mathbf{b}=(b_1, b_2, \cdots, b_m)$ with length m. The message sequence can be firstly encrypted by applying the bitwise XOR operation with a pseudo-random sequence to ensure security. The pseudo-random sequence is generated by a data hiding key using the stream cipher Spritz. The data embedding algorithm is described as follows.

- *Case 1*: If $z_{ij} > T_p$ or $z_{ij} < T_n$, shift z_{ij} by 1 unit to the right or the left respectively.

$$z'_{ij} = \begin{cases} z_{ij}+1 & \text{if } z_{ij} > T_p \\ z_{ij}-1 & \text{if } z_{ij} < T_n \end{cases} \tag{20}$$

  where z_{ij} is the (i,j)th original encrypted quantized DCT coefficient in the 4×4 block and z'_{ij} is the corresponding stego coefficient.
- *Case 2*: If $z_{ij}=T_p$ or $z_{ij}=T_n$, modify z_{ij} according to the to-be-embedded message bit.

[4] We say “estimate” because the rounding operator on DCT coefficients may cause rounding errors. However, rounding errors do not disturb our discussion. In practice, we just need to sort embedding distortions caused by modifying coefficients in different coordinates.

[5] In each stego video, only one coefficient classification is used for data embedding.

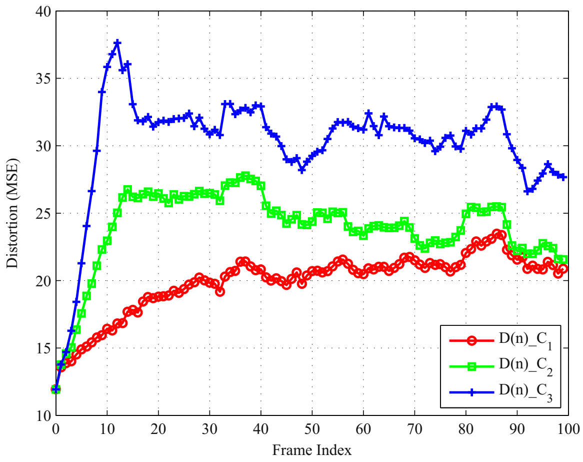

Fig. 4. Overall distortion comparison.

$$z'_{ij} = \begin{cases} z_{ij} & \text{if } z_{ij} = T_p \text{ and } b_k = 0 \\ z_{ij} + 1 & \text{if } z_{ij} = T_p \text{ and } b_k = 1 \\ z_{ij} & \text{if } z_{ij} = T_n \text{ and } b_k = 0 \\ z_{ij} - 1 & \text{if } z_{ij} = T_n \text{ and } b_k = 1 \end{cases} \tag{21}$$

- *Case 3*: If $T_n < z_{ij} < T_p$, z_{ij} remains unchanged.

$$z'_{ij} = z_{ij} \tag{22}$$

Using the above data embedding algorithm, the data hider should do the following steps to complete data embedding.

- *Step 1*: Partial decoding is performed on the encrypted video bitstream to obtain the encrypted quantized luma DCT coefficients. The data embedding starts in the *N*th frame.
- *Step 2*: Embed message bits into inter-coded macroblocks (excluding P_Skip mode coded macroblocks) within the current frame using coefficient selection, i.e., embedding data into the coefficients in C_1 with highest priority, the coefficients in C_2 with medium priority and the coefficients in C_3 with lowest priority. During data embedding process, record the number of embedded message bits *k*.
- *Step 3*: If $k < m$, go back to *Step 2* for embedding data in previous frames one by one until all message bits have been embedded.
- *Step 4*: Partial encoding is performed on the encrypted quantized luma DCT coefficients to regenerate the encrypted video bitstream.

If there exist multiple GOPs in the video, we can complete data embedding using similar steps. For the last GOP, the data embedding starts in the last frame and proceeds to previous frames one by one. If the last GOP cannot contain all message bits, go back to previous GOPs for data embedding until all message bits have been embedded. The number of embedded message bits *m* in each given video bitstream should be stored by the data hider for data extraction.

2.3. Data extraction and video recovery

In the proposed scheme, the embedded data can be extracted either in the encrypted domain or in the decrypted domain. The order of video decryption and data extraction implies two different application scenarios.

2.3.1. Data extraction in the encrypted domain

In this application scenario, in order to protect the confidentiality of video content, the cloud server does not have sufficient authority to access video content due to absence of the encryption key. Therefore, it is necessary for the cloud server to extract the embedded authentication data in the encrypted domain to manage the video.

Before data extraction in the encrypted domain, partial decoding is performed on the encrypted video bitstream to obtain the encrypted quantized luma DCT coefficients. The embedded data can be extracted from two zones, which are $Z_p = [T_p, T_p + 1]$ and $Z_n = [T_n - 1, T_n]$. The data extraction is the inverse process of data embedding. We can extract the embedded message sequence $\mathbf{b} = (b_1, b_2, \cdots, b_m)$ as depicted in Eq. (23).

$$b_k = \begin{cases} 0 & \text{if } z'_{ij} \in Z_p \text{ and } \operatorname{mod}(z'_{ij} - T_p, 2) = 0 \\ 1 & \text{if } z'_{ij} \in Z_p \text{ and } \operatorname{mod}(z'_{ij} - T_p, 2) = 1 \\ 0 & \text{if } z'_{ij} \in Z_n \text{ and } \operatorname{mod}(T_n - z'_{ij}, 2) = 0 \\ 1 & \text{if } z'_{ij} \in Z_n \text{ and } \operatorname{mod}(T_n - z'_{ij}, 2) = 1 \end{cases} \tag{23}$$

where z'_{ij} is the (i,j)th stego quantized DCT coefficient in the 4 × 4 block. The original encrypted quantized DCT coefficient recovery is described as follows.

- *Case 1*: If $z'_{ij} \in [T_p, T_p + 1]$ or $z'_{ij} \in [T_n - 1, T_n]$, the original encrypted quantized DCT coefficient can be losslessly recovered by

$$z_{ij} = \begin{cases} z'_{ij} & \text{if } z'_{ij} \in Z_p \text{ and } \operatorname{mod}(z'_{ij} - T_p, 2) = 0 \\ z'_{ij} - 1 & \text{if } z'_{ij} \in Z_p \text{ and } \operatorname{mod}(z'_{ij} - T_p, 2) = 1 \\ z'_{ij} & \text{if } z'_{ij} \in Z_n \text{ and } \operatorname{mod}(T_n - z'_{ij}, 2) = 0 \\ z'_{ij} + 1 & \text{if } z'_{ij} \in Z_n \text{ and } \operatorname{mod}(T_n - z'_{ij}, 2) = 1 \end{cases} \tag{24}$$

- *Case 2*: If $z'_{ij} > T_p + 1$ or $z'_{ij} < T_n - 1$, shift z'_{ij} by 1 unit to the center.

$$z_{ij} = \begin{cases} z'_{ij} - 1 & \text{if } z'_{ij} > T_p + 1 \\ z'_{ij} + 1 & \text{if } z'_{ij} < T_n - 1 \end{cases} \tag{25}$$

- *Case 3*: If $T_n < z'_{ij} < T_p$, z_{ij} is equal to z'_{ij}.

$$z_{ij} = z'_{ij} \tag{26}$$

Since the data embedding process is reversible, the content owner can decrypt the encrypted video to obtain the original video with the encryption key.

2.3.2. Data extraction in the decrypted domain

In this application scenario, the receiver may download the video from the cloud server and view the decrypted reconstructed video using the encryption key. The decrypted video still contains the embedded authentication data, which is convenient for the cloud server to manage the video. If the content owner does not want to upload the video, he/she can extract the embedded data after video decryption. Our proposed inter-frame distortion drift prevention scheme can improve the quality of the reconstructed video containing embedded data. The entire process is composed of the following steps.

- *Step 1*: Generate the marked decrypted video with the encryption key. Due to the symmetry of the bitwise XOR operation, the decryption operation is symmetric to the encryption operation.
- *Step 2*: Extract the embedded data and recover the original video losslessly. Because the video encryption scheme only changes the signs of quantized DCT coefficients, this step can be performed similarly using Eqs. (23)–(26).

Since the data embedding process is reversible, the original video can be obtained with the encryption key.

3. Experimental results

The proposed scheme for reversible data hiding in encrypted H.264/AVC video bitstreams has been integrated into the H.264/AVC reference software JM 10.2 [26]. Besides, the schemes proposed by Gujjunoori et al. [15], Bouchama et al. [16] and Xu et al. [20] are implemented for performance comparison. The histogram shifting technique [21] is used in Xu et al.'s scheme and our proposed scheme for data embedding. As shown in Fig. 5, eight video sequences (i.e., Carphone, Coastguard, Container, Foreman, Hall, Harbor, Mobile, and Salesman) in QCIF format [25] are used in the experiments. The first 100 frames of each video sequence are encoded at frame rate 30 fps. The GOP (Group of Picture) structure is IPPP, in which only the first frame of each video sequence is encoded as an I-frame and the remaining frames are encoded as P-frames.

3.1. Security of the encryption scheme

For the video encryption scheme, the security includes the cryptographic security and the perception security.

Cryptographic security: Cryptographic security means that the encryption scheme can resist cryptographic attacks, which depends on the adopted ciphers. In the encryption scheme, the novel stream cipher Spritz [22], which is an improved variant of the stream cipher RC4, is used to encrypt the key coding parameters and the authentication data. It is estimated that Spritz can produce output with about 24 cycles/byte of computation. Furthermore, it is suggested that about 2^{81} bytes of output are needed before reasonably distinguishing Spritz output from random sequence. This is a significant improvement over RC4 [22].

Perception security: Perception security means that the encryption scheme can keep the encrypted video unintelligible. The intra prediction modes (IPM), the motion vector differences (MVD) and the residual coefficients are selectively encrypted in the proposed scheme. In our experiments, QP is set as 28 to generate the video bitstream. The scrambling effect of encrypted video frames is given in Fig. 6. The luma PSNR values of encrypted video frames compared with the original video frames are 11.27 dB, 9.51 dB, 10.79 dB, 10.17 dB, 9.66 dB, 9.54 dB, 9.61 dB and 13.08 dB respectively. Compared with the original video frames in Fig. 5, it is difficult to recognize the contents of encrypted frames. Due to the space limitation, we do not list the encrypted results of all frames. Other frames in each given video sequence have the similar scrambling effect. The scrambling effect can be more obvious if the video content contains intense motion and complex texture. For example, the contents of video sequences Harbor and Mobile are totally distorted. However, there exist a large number of P_Skip mode coded macroblocks in P-frames for encoding video sequences with slight motion. For this coding mode, neither motion vectors nor residual coefficients are transmitted. It means that encrypting motion vectors and residual coefficients has no scrambling effect on the P_Skip macroblocks. For video sequences with slight motion, the perception security of encrypted frames mainly depends on the scrambling effect of corresponding I-frames. Therefore, the scrambling effect of video sequences Hall and Salesman is relatively weaker.

3.2. Visual quality of the stego video

In our experiments, we use commonly adopted measurements PSNR and SSIM [29] to evaluate the objective visual quality of stego videos. The PSNR (dB) and the SSIM are calculated by comparing the decoded reconstructed video sequence with the original video sequence. In the proposed scheme, the embedding capacity C is the sum of the number of bin 1 and the number of bin -1, which are the two highest bins in the histogram of quantized DCT coefficients. (Zero coefficients are not used for data embedding.) In Xu et al.'s scheme [20], the scale factor β is used for choosing the actual data embedding zone and adjusting the embedding capacity. We set β as 0 to guarantee that Xu et al.'s scheme and our proposed scheme have the same embedding capacity at the same coding setting for fair comparison. The embedding rate γ" and "can be defined as the ratio of the number of actual embedded message bits m to the embedding capacity C.

To evaluate the visual quality of the stego videos, we first decrypt the encrypted videos containing embedded data using the encryption key. The comparison of average luma PSNR (dB) and average luma SSIM between Xu et al.'s scheme and our proposed scheme at embedding rate 50% using different QP values is listed in Table 2, in which the embedding capacity of each video is given. The visual quality of cover videos without embedded data is also

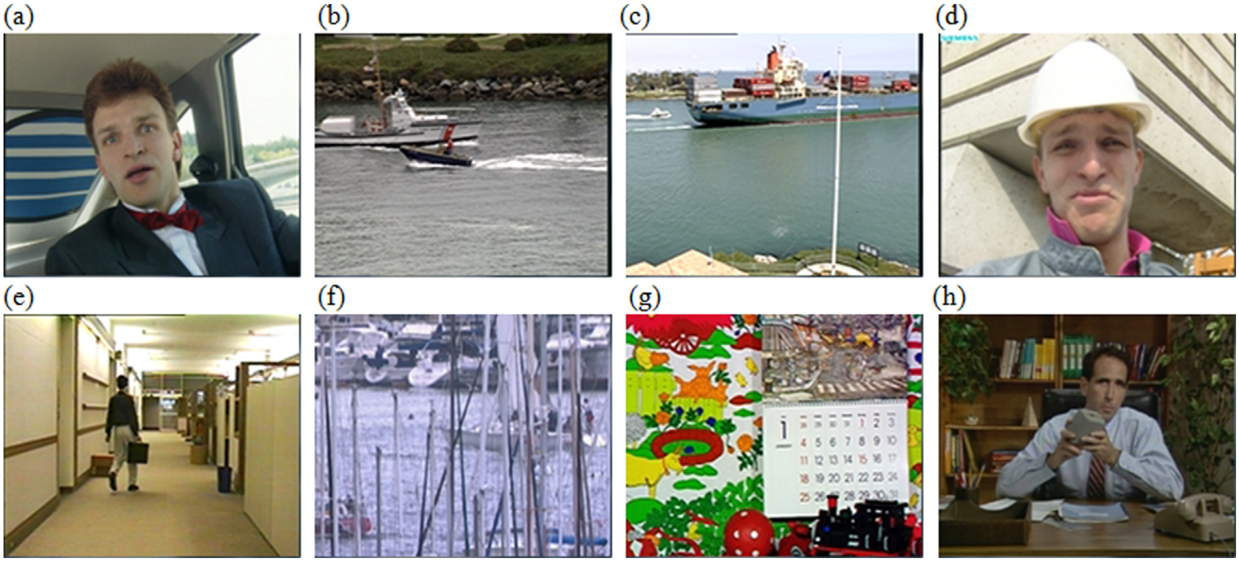

Fig. 5. Video sequences used in the experiments. (a) Carphone, (b) Coastguard, (c) Container, (d) Foreman, (e) Hall, (f) Harbor, (g) Mobile, and (h) Salesman.

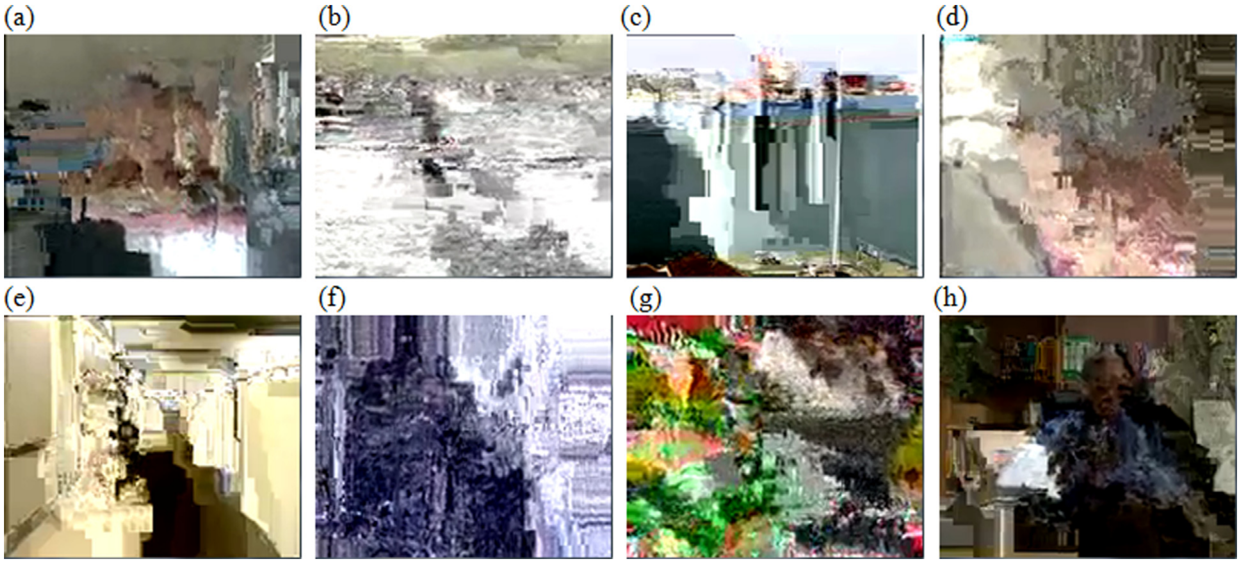

Fig. 6. Encrypted video frames. (a) Carphone, (b) Coastguard, (c) Container, (d) Foreman, (e) Hall, (f) Harbor, (g) Mobile, and (h) Salesman.

presented in Table 2. The bold digits in Table 2 mean that the corresponding scheme can achieve better visual quality of stego videos. The embedding capacity depends on the video content and the QP value. Using the same QP, the embedding capacity of the video with intense motion and complex texture is larger because the number of non-zero quantized DCT coefficients is larger. For instance, the embedding capacity of video sequence Mobile is obviously larger than that of video sequence Salesman. For each given video, the embedding capacity decreases with the increasing of QP value because coarser quantization will generate more zero quantized DCT coefficients. Our proposed scheme focuses on decreasing the inter-frame distortion drift so that it outperforms Xu et al.'s scheme in terms of average luma PSNR and average luma SSIM. Moreover, the superiority on average luma PSNR is more obvious when the QP is smaller. For video sequence Carphone, our proposed scheme outperforms Xu et al.'s scheme in terms of average luma PSNR by 1.30 dB, 1.89 dB and 3.31 dB using QP 32, QP 28 and QP 24 respectively.

To compare the objective visual quality of decrypted stego videos among Gujjunoori et al.'s scheme [15], Bouchama et al.'s scheme [16], Xu et al.'s scheme [20] and our proposed scheme, we illustrate the curves of average luma PSNR values at five different embedding rates using QP 28 in Fig. 7. To calibrate the embedding rate among these four schemes, we denote the embedding rate γ and as the ratio of the number of actual embedded message bits m to the sum of the number of bin 1 and the number of bin -1. Gujjunoori et al.'s

Table 2
Comparison of average luma PSNR (dB) and average luma SSIM at embedding rate 50% using different QP values.

Video sequence	Quantization parameter	Embedding capacity	PSNR (dB)			SSIM		
			Cover	Xu et al. [20]	Proposed	Cover	Xu et al. [20]	Proposed
Carphone	24	52,355	39.89	33.49	**36.80**	0.9800	0.9616	**0.9680**
	28	22,915	36.95	33.10	**34.99**	0.9667	0.9536	**0.9584**
	32	8934	33.98	31.42	**32.72**	0.9461	0.9338	**0.9385**
Coastguard	24	200,428	37.12	26.94	**33.12**	0.9634	0.8615	**0.9329**
	28	92,213	33.94	26.18	**31.18**	0.9246	0.8312	**0.8999**
	32	31,162	30.89	25.38	**29.21**	0.8541	0.7821	**0.8397**
Container	24	26,131	38.71	34.91	**37.26**	0.9571	0.9455	**0.9529**
	28	9887	36.05	34.02	**35.40**	0.9403	0.9357	**0.9390**
	32	3389	33.38	32.49	**33.10**	0.9258	0.9231	**0.9250**
Foreman	24	60,827	38.86	31.00	**35.97**	0.9759	0.9424	**0.9634**
	28	29,686	36.15	30.17	**34.04**	0.9613	0.9321	**0.9502**
	32	14,221	33.42	28.71	**31.84**	0.9376	0.9073	**0.9265**
Hall	24	24,700	39.84	34.51	**37.87**	0.9794	0.9683	**0.9769**
	28	13,461	37.35	32.99	**35.97**	0.9726	0.9611	**0.9703**
	32	7252	34.51	31.50	**33.53**	0.9588	0.9471	**0.9563**
Harbor	24	295,230	36.95	27.24	**31.97**	0.9852	0.9304	**0.9525**
	28	160,100	33.65	25.48	**29.46**	0.9684	0.9008	**0.9300**
	32	67,074	30.27	24.54	**27.32**	0.9312	0.8705	**0.8954**
Mobile	24	329,938	36.70	24.73	**31.63**	0.9878	0.9104	**0.9614**
	28	169,418	33.13	24.27	**29.74**	0.9737	0.9012	**0.9521**
	32	65,460	29.42	23.96	**27.51**	0.9420	0.8848	**0.9254**
Salesman	24	25,661	38.62	33.16	**35.80**	0.9769	0.9596	**0.9676**
	28	12,378	35.60	31.59	**33.59**	0.9546	0.9370	**0.9464**
	32	5600	32.55	30.13	**31.38**	0.9091	0.8937	**0.9022**

scheme and Bouchama et al.'s scheme cannot achieve high average luma PSNR values because the embedded message bits are largely located in the first few P-frames and the embedding distortion tends to accumulate rapidly. It can be observed that our proposed scheme outperforms other three schemes at five embedding rates. The superiority is more notable if the video content contains intense motion because the inter-frame distortion drift is severer in such video. For video sequence Mobile, our proposed scheme outperforms Gujjunoori et al.'s scheme, Bouchama et al.'s scheme and Xu et al.'s scheme in terms of average luma PSNR by 15.36 dB, 15.11 dB and 5.75 dB respectively at embedding rate 10%. For video sequence Hall, our proposed scheme outperforms Gujjunoori et al.'s scheme, Bouchama et al.'s scheme and Xu et al.'s scheme in terms of average luma PSNR by 9.87 dB, 9.70 dB and 2.47 dB respectively at embedding rate 10%. Through the comparisons in Table 2 and Fig. 7, we can infer that our proposed inter-frame distortion drift prevention scheme is effective in improving the objective visual quality of stego videos.

To explore the effect of our proposed inter-frame distortion drift prevention scheme on the video quality of each frame, we give the comparison of the luma PSNR values of first 100 decoded frames of video sequence Foreman at embedding rate 50% using QP 28 in Fig. 8. It can be seen from Fig. 8 that our proposed scheme can achieve the best visual quality for the following two reasons. Firstly, the coefficient selection in our proposed scheme aims to decrease the embedding distortion in each P-frame. Secondly, data embedding starts in the last frame in each GOP and then proceeds to previous frames one by one to decrease the embedding distortion accumulation in our proposed scheme. Fig. 9 shows the subjective results of the 1st frame, 16th frame, 31st frame, 46th frame, and 61st frame of video sequence Foreman using the same coding setting in Fig. 8. The first frame is an I-frame without containing embedded data. Gujjunoori et al.'s scheme and Bouchama et al.'s scheme cause obvious distortion as depicted in Fig. 9. The subjective visual quality in our proposed scheme is better than that in Gujjunoori et al.'s scheme, Bouchama et al.'s scheme and Xu et al.'s scheme.

3.3. *Impacts on the compression efficiency*

Data embedding can change the probability distribution of original residual coefficients. As a result, the number of bits used in the stego compressed video will increase compared with that in the cover compressed video. After the cloud server embeds the authentication data into the encrypted video bitstream, the bit rate increment will consume the storage resources. This is not appreciated. To further evaluate the performance of the proposed scheme, the video bit rate increment BR_{inc} caused by data embedding is also compared.

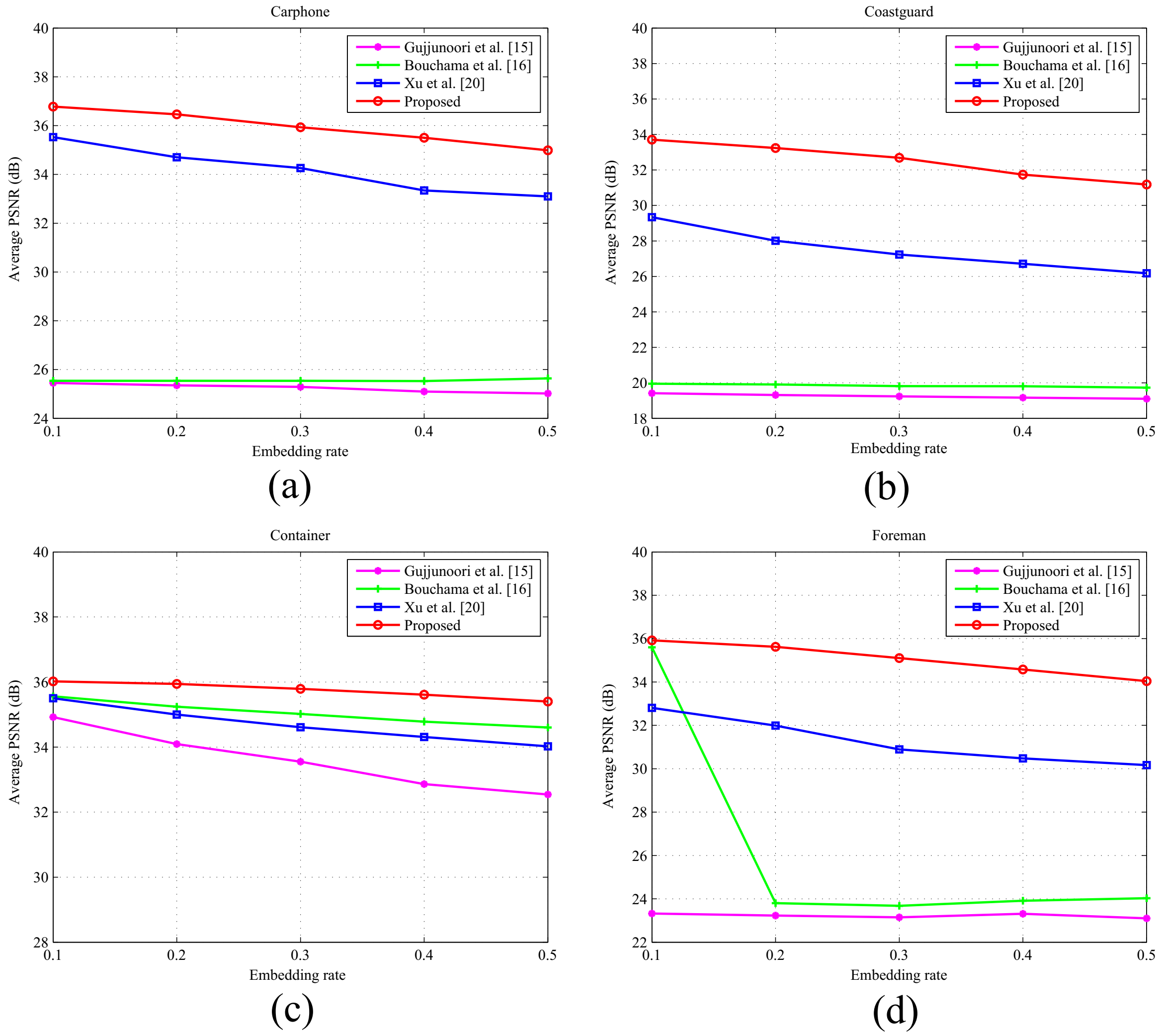

(a)

(b)

(c)

(d)

Fig. 7. Comparison of average luma PSNR (dB) at five embedding rates using QP 28. (a) Carphone, (b) Coastguard, (c) Container, (d) Foreman, (e) Hall, (f) Harbor, (g) Mobile, and (h) Salesman.

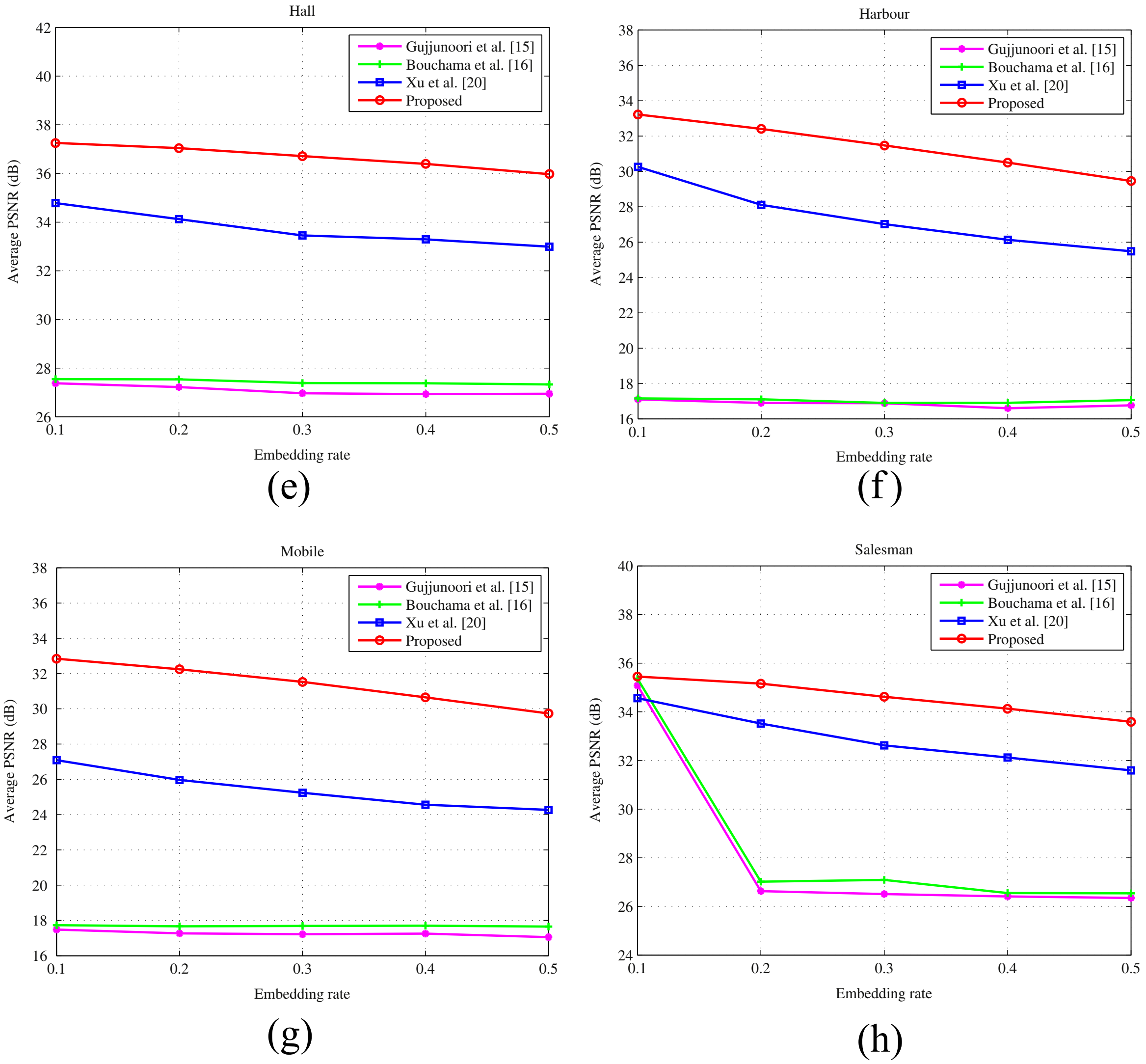

(e)

(f)

(g)

(h)

Fig. 7. (*continued*)

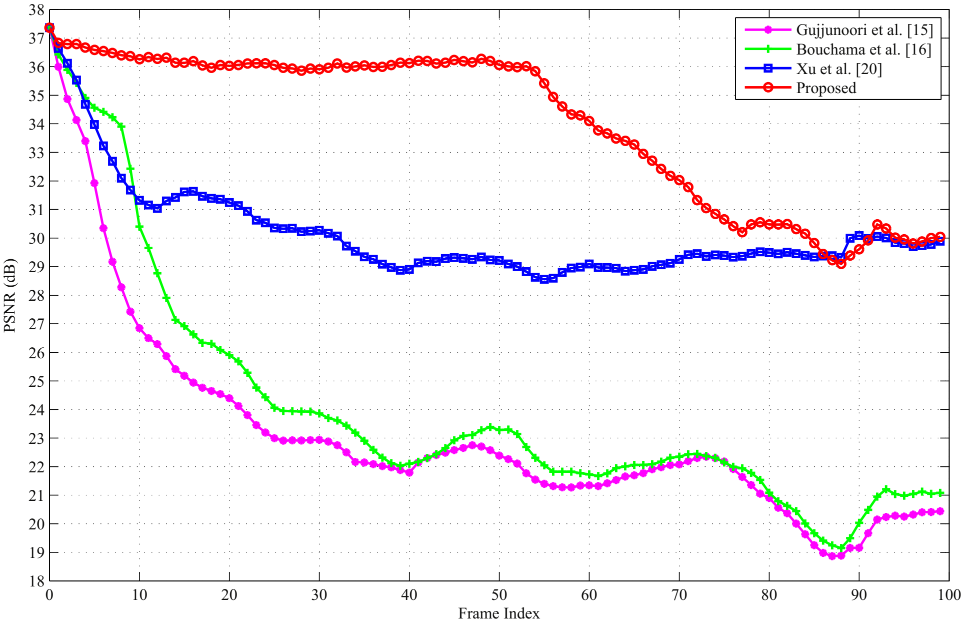

Fig. 8. Comparison of luma PSNR values of first 100 decoded frames of video sequence Foreman at embedding rate 50% using QP 28.

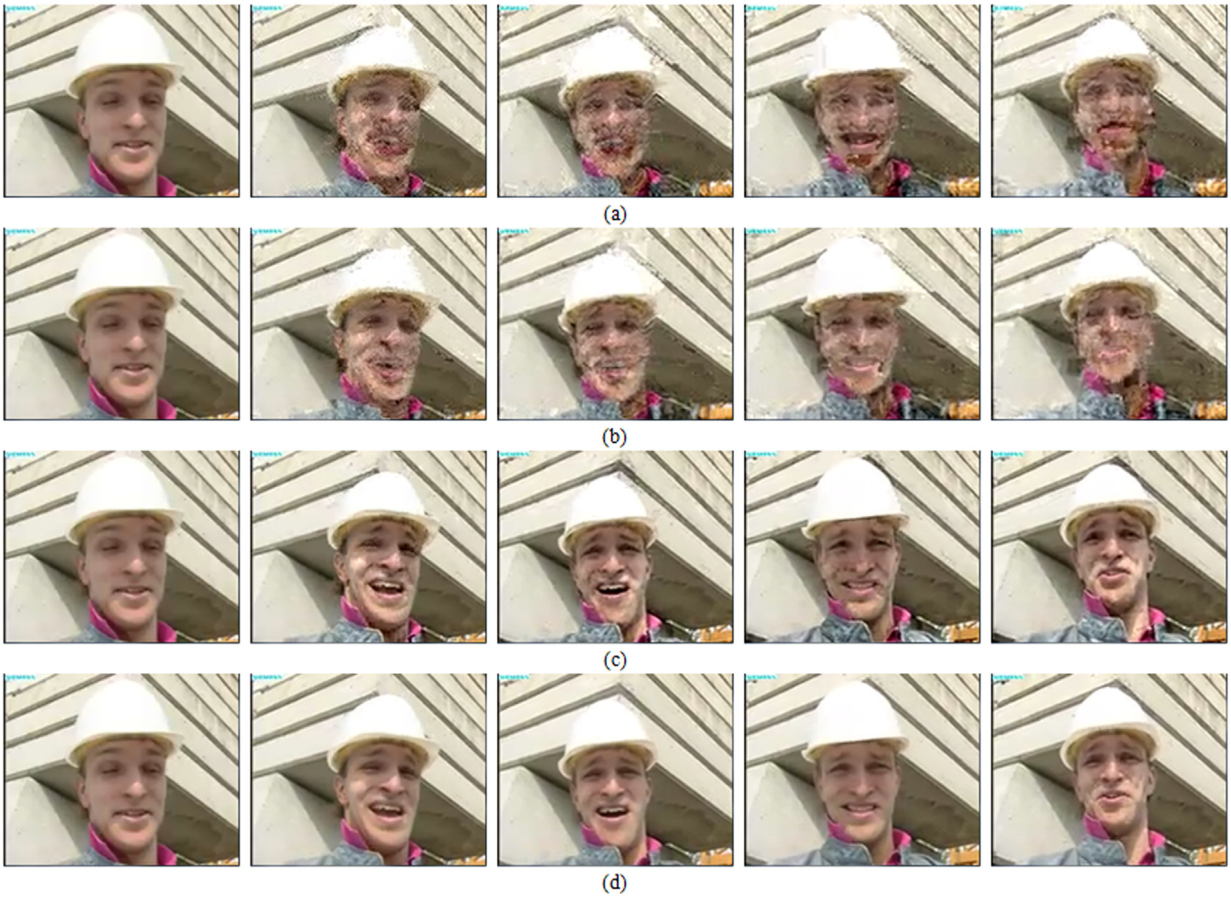

Fig. 9. Subjective results of video sequence Foreman at embedding rate 50% using QP 28. (a) Gujjunoori et al. [15], (b) Bouchama et al. [16], (c) Xu et al. [20], and (d) proposed.

$$BR_{inc} = \frac{BR_{stg} - BR_{org}}{BR_{org}} \times 100\% \tag{27}$$

where BR_{org} is the video bit rate of the original compressed video bitstream and BR_{stg} is the video bit rate of the stego compressed video bitstream. The comparison of video bit rate increments among Gujjunoori et al.'s scheme [15], Bouchama et al.'s scheme [16], Xu et al.'s scheme [20] and our proposed scheme at five embedding rates using QP 28 is listed in Table 3, in which can be seen that the video bit rate increases as the embedding rate increases. The bold digits in Table 3 mean that the corresponding scheme can achieve the smallest video bit rate increment. In CAVLC-based entropy coding, modifying zero quantized DCT coefficients can considerably increase the video bit rate. To avoid this problem, zero quantized DCT coefficients are not modified during data embedding in Xu et al.'s scheme and our proposed scheme. Therefore, the video bit rate increments in both schemes can maintain in an acceptable range. However, Gujjunoori et al.'s scheme and Bouchama et al.'s scheme modify zero quantized DCT coefficients for data embedding, so the video bit rate increments are larger in most cases.

3.4. *Discussion of the robustness*

The robustness is a beneficial property in video data hiding. With robustness, video data hiding methods can resist some attacks, such as packet loss and recompression. To enhance the robustness of our proposed scheme, error control codes should be used [30,31]. In our experiments, the plain message bits are encoded using BCH (n, k, t) codes [32] in which $n/k = 7/4$ and $t=1$ to generate the actual to-be-embedded message bits before data embedding. The word plain is associated with the original message bits which need to be transmitted. Given the embedding capacity C, a total of C_p plain message bits can be embedded, where $C_p = \lfloor C \cdot k/n \rfloor$. We use the survival rate to evaluate the robustness of our proposed scheme. The survival rate is defined as the ratio of the number of correctly extracted message bits to the number of actual embedded message bits.

To compare the robustness against packet loss, the stego videos are generated using our proposed scheme with and without BCH (7, 4, 1) codes respectively. Table 4 presents the robustness against packet loss of video sequence Foreman at embedding rate 50%. It can be seen that the survival rate decreases as the packet loss rate increases using certain QP value. The BCH codes can enhance the robustness of our proposed scheme against packet loss.

To compare the robustness against recompression, we first generate stego videos using our proposed scheme with and without BCH (7, 4, 1) codes respectively when QP is certain. Afterwards, the stego videos are decompressed and recompressed using a range of QP values. Table 5 presents the robustness against recompression of video sequence Foreman at embedding rate 50%. Without BCH codes, the survival rate gets close to 50%. It means that the robustness of our proposed scheme against recompression is very weak without error control. Fortunately, BCH codes can enhance the robustness. With BCH codes, the survival rate can be obviously improved. The BCH codes enhance the robustness at the cost of decreasing the number of embedded plain message bits at given embedding rate. In the actual application scenario, we can adjust the BCH codes and the embedding rate to obtain a tradeoff between the robustness and the number of embedded plain

Table 3
Comparison of video bit rate increments at five embedding rates using QP 28.

Embedding rate (%)	Scheme	Carphone (%)	Coastguard (%)	Container (%)	Foreman (%)	Hall (%)	Harbor (%)	Mobile (%)	Salesman (%)
10	Gujjunoori et al. [15]	2.883	4.381	2.876	2.846	3.217	4.697	4.063	2.599
	Bouchama et al. [16]	1.666	2.317	1.444	**1.398**	2.007	2.629	2.235	1.385
	Xu et al. [20]	**1.187**	2.113	1.407	1.428	1.301	2.063	1.678	1.299
	Proposed	1.276	**2.017**	**1.383**	1.445	**1.193**	**2.044**	**1.652**	**1.239**
20	Gujjunoori et al. [15]	5.382	8.359	5.587	5.918	6.301	8.566	7.764	5.098
	Bouchama et al. [16]	2.949	4.506	2.894	**2.677**	3.472	4.935	4.261	2.913
	Xu et al. [20]	**2.399**	4.214	2.815	2.769	2.679	4.114	3.362	2.659
	Proposed	2.579	**4.051**	**2.674**	2.802	**2.416**	**4.109**	**3.298**	**2.590**
30	Gujjunoori et al. [15]	7.883	12.324	8.573	8.662	10.014	12.017	11.059	7.792
	Bouchama et al. [16]	4.282	**5.869**	4.400	4.226	5.186	6.803	6.246	7.942
	Xu et al. [20]	**3.643**	6.287	4.326	**4.115**	4.023	**6.179**	5.044	3.980
	Proposed	3.894	6.057	**4.094**	4.189	**3.588**	6.182	**4.942**	**3.950**
40	Gujjunoori et al. [15]	10.453	16.752	11.314	10.804	12.495	15.922	14.370	10.300
	Bouchama et al. [16]	5.631	8.354	5.801	**5.384**	6.637	8.724	8.001	7.026
	Xu et al. [20]	**4.905**	8.400	5.703	5.472	5.173	**8.237**	6.711	5.236
	Proposed	5.208	**8.095**	**5.489**	5.602	**4.725**	8.252	**6.607**	**5.210**
50	Gujjunoori et al. [15]	13.083	20.221	14.025	13.889	14.472	19.805	18.027	13.023
	Bouchama et al. [16]	7.523	10.317	7.178	7.067	7.787	10.910	9.548	9.340
	Xu et al. [20]	**6.222**	10.462	7.031	**6.808**	6.474	10.288	8.375	6.553
	Proposed	6.487	**10.112**	**6.854**	6.993	**5.940**	**10.270**	**8.269**	**6.527**

Table 4
Robustness against packet loss of video sequence Foreman at embedding rate 50%.

Quantization parameter for stego video	Packet loss rate (%)	Survival rate without BCH (%)	Survival rate with BCH (%)
24	10	95.104	97.340
	20	90.050	94.519
	30	85.388	92.050
	40	80.311	89.297
	50	75.458	87.022
28	10	95.203	97.305
	20	90.009	94.442
	30	85.414	92.225
	40	80.314	89.254
	50	75.349	86.970
32	10	95.176	97.468
	20	89.873	94.627
	30	84.852	91.758
	40	80.295	89.437
	50	76.104	87.032

Table 5
Robustness against recompression of video sequence Foreman at embedding rate 50%.

Quantization parameter for stego video	Quantization parameter for recompression	Survival rate without BCH (%)	Survival rate with BCH (%)
24	20	49.946	73.067
	22	49.755	73.025
	24	50.337	73.314
	26	50.248	73.192
	28	50.199	73.498
28	24	50.381	73.139
	26	50.563	73.718
	28	50.408	73.307
	30	49.943	73.429
	32	50.286	73.368
32	28	51.210	73.755
	30	53.572	74.782
	32	49.311	72.841
	34	49.747	72.813
	36	49.536	72.644

message bits.

4. Conclusion and future work

In this paper, an effective scheme for reversible data hiding in encrypted H.264/AVC video bitstreams is proposed. In the encryption phase, three types of key coding parameters including the intra prediction modes, the motion vector differences and the quantized DCT coefficients are selectively encrypted without video bit rate increment for preserving the confidentiality of video content. In the data hiding phase, we present a theoretical analysis of the inter-frame distortion drift for alleviating the video quality degradation due to data embedding. Based on the analysis, we estimate the embedding distortions caused by modifying different residual coefficients and embed data into residual coefficients with different priorities for decreasing the inter-frame distortion drift. The data embedding is implemented by the histogram shifting technique. The embedded data can be extracted either in the encrypted domain or in the decrypted domain for meeting different application scenarios. If the receiver decrypts the encrypted video bitstream and extracts the embedded data, the original video bitstream can be perfectly recovered. In addition, if the receiver decrypts the encrypted video bitstream without extracting the embedded data, the bitstream can still be decoded to obtain the reconstructed video with good quality.

In reversible video data hiding, how to determine the optimal modification of quantized DCT coefficients for obtaining best visual quality and compression efficiency at given embedding rate is still a challenging problem. In the future, a comprehensive reversible video data hiding scheme using rate-distortion optimization deserves further investigation.

Acknowledgments

This work was supported in part by the National Natural Science Foundation of China under Grants 61572452 and 61170234, in part by the Strategic Priority Research Program of the Chinese Academy of Sciences under Grant XDA06030601, and in part by the China Scholarship Council Program under Grant 201506340006. The authors would like to sincerely thank the editors and the anonymous reviewers for their valuable comments.

Appendix A

This appendix is to verify that the assumption $\mathrm{E}\{[\tilde{F}(n-1,j)-\hat{F}(n-1,j)][\tilde{r}(n,i)-\hat{r}(n,i)]\}=0$ in Eq. (6), where pixel j is the motion prediction of pixel i.

To facilitate understanding, we first provide some explanations for some key variables. Let $F(n-1,j)$ be the original luma value of pixel j in the $(n-1)$th video frame and $\hat{F}(n-1,j)$ be the reconstructed luma value of pixel j in the feedback loop at the encoder. We denote the reconstructed luma value of pixel j at the receiver end as $\tilde{F}(n-1,j)$. $\tilde{F}(n-1,j)$ may be different from $\hat{F}(n-1,j)$ due to data embedding. For inter-coded macroblocks, let $r(n,i)$ be the motion compensation residue at the encoder. Let $\tilde{r}(n,i)$ and $\hat{r}(n,i)$ be the corresponding reconstructed values with embedded data and without embedded data respectively. According to motion compensation, we can rewrite $\tilde{F}(n-1,j)-\hat{F}(n-1,j)$ as follows.

$$\begin{aligned}
&\tilde{F}(n-1,j)-\hat{F}(n-1,j)\\
&\quad=[\tilde{F}(n-2,j_{n-2})+\tilde{r}(n-1,i_{n-1})]\\
&\qquad-[\hat{F}(n-2,j_{n-2})+\hat{r}(n-1,i_{n-1})]\\
&\quad=[\tilde{F}(n-2,j_{n-2})-\hat{F}(n-2,j_{n-2})]\\
&\qquad+[\tilde{r}(n-1,i_{n-1})-\hat{r}(n-1,i_{n-1})]\\
&\quad=[\tilde{F}(n-3,j_{n-3})-\hat{F}(n-3,j_{n-3})]\\
&\qquad+\sum_{k=1}^{2}[\tilde{r}(n-k,i_{n-k})-\hat{r}(n-k,i_{n-k})]\\
&\quad=[\tilde{F}(1,j_1)-\hat{F}(1,j_1)]+\sum_{k=1}^{n-2}[\tilde{r}(n-k,i_{n-k})-\hat{r}(n-k,i_{n-k})]\\
&\quad=\sum_{k=1}^{n-2}[\tilde{r}(n-k,i_{n-k})-\hat{r}(n-k,i_{n-k})]
\end{aligned}\tag{28}$$

where pixel j_{k-1} is the motion prediction of pixel i_k. The fifth identity in Eq. (28) is based on the condition that the first I-frame is not used for data embedding, i.e., $\tilde{F}(1,j_1)=\hat{F}(1,j_1)$. After motion compensation, the residues tend to be less correlated [27]. We can rewrite $\mathrm{E}\{[\tilde{F}(n-1,j)-\hat{F}(n-1,j)][\tilde{r}(n,i)-\hat{r}(n,i)]\}$ as follows.

$$\begin{aligned}
&\mathrm{E}\{[\tilde{F}(n-1,j)-\hat{F}(n-1,j)][\tilde{r}(n,i)-\hat{r}(n,i)]\}\\
&\quad=\mathrm{E}\left\{\sum_{k=1}^{n-2}[\tilde{r}(n-k,i_{n-k})-\hat{r}(n-k,i_{n-k})][\tilde{r}(n,i)-\hat{r}(n,i)]\right\}\\
&\quad=\sum_{k=1}^{n-2}\mathrm{E}\{[\tilde{r}(n-k,i_{n-k})-\hat{r}(n-k,i_{n-k})][\tilde{r}(n,i)-\hat{r}(n,i)]\}\\
&\quad=\sum_{k=1}^{n-2}\mathrm{E}\{\tilde{r}(n-k,i_{n-k})-\hat{r}(n-k,i_{n-k})\}\cdot\mathrm{E}\{\tilde{r}(n,i)-\hat{r}(n,i)\}
\end{aligned}\tag{29}$$

Therefore, we just need to verify that the difference between the reconstructed residue $\tilde{r}(n,i)$ with embedded data and the reconstructed residue $\hat{r}(n,i)$ without embedded data has zero mean, i.e., $\mathrm{E}\{\tilde{r}(n,i)-\hat{r}(n,i)\}=0$.

We can estimate the error matrix E of the pixel luma value between the reconstructed residual block $\tilde{R}$ with embedded data and the reconstructed residual block $\hat{R}$ without embedded data in Eq. (16) as follows.

$$\begin{aligned}
&E=\tilde{R}-\hat{R}\\
&=\mathrm{round}[C_i^T(Z.\times Qstep.\times PF)C_i+C_i^T(\triangle.\times Qstep.\times PF)C_i]\\
&\quad-\mathrm{round}[C_i^T(Z.\times Qstep.\times PF)C_i]\\
&\approx C_i^T(\triangle.\times Qstep.\times PF)C_i
\end{aligned}\tag{30}$$

where $\triangle=(\delta_{ij})_{4\times4}$ is the error matrix added to the quantized DCT coefficient matrix Z in the 4×4 block. If the message bit in the binary message sequence $\mathbf{b}=(b_1,b_2,\cdots,b_m)$ is uniformly distributed and the histogram shifting technique is used as depicted in Eqs. (20)–(22), we have $\mathrm{E}\{\delta_{ij}\}=0$. Therefore, $\mathrm{E}\{\tilde{r}(n,i)-\hat{r}(n,i)\}\approx0$ and the assumption in Eq. (6) has been verified.

References

[1] A.J. Menezes, P.C. van Oorschot, S.A. Vanstone, Handbook of Applied Cryptography, CRC Press, Boca Raton, Florida, 1996.

[2] T. Wiegand, G.J. Sullivan, G. Bjontegaard, A. Luthra, Overview of the H.264/AVC video coding standard, IEEE Trans. Circuits Syst. Video Technol. 13 (7) (2003) 560–576.

[3] J. Ahn, H.J. Shim, B. Jeon, I. Choi, Digital video scrambling method using intra prediction mode, in: Proceedings of 5th Pacific Rim Conference on Multimedia, 2004, pp. 386–393.

[4] J. Jiang, Y. Liu, Z. Su, G. Zhang, S. Xing, An improved selective encryption for H.264 video based on intra prediction mode scrambling, J. Multimed. 5 (5) (2010) 464–472.

[5] S. Lian, Z. Liu, Z. Ren, Z. Wang, Selective video encryption based on advanced video coding, in: Proceedings of 6th Pacific Rim Conference on Multimedia, 2005, pp. 281–290.

[6] S. Lian, Z. Liu, Z. Ren, H. Wang, Secure advanced video coding based on selective encryption algorithms, IEEE Trans. Consum. Electron. 52 (2) (2006) 621–629.

[7] T. Shi, B. King, P. Salama, Selective encryption for H.264/AVC video coding, in: Proceedings of SPIE Security, Steganography, and Watermarking of Multimedia Contents VIII, 2006, pp. 607217-1–607217-9.

[8] X. Zhang, Reversible data hiding in encrypted images, IEEE Signal Process. Lett. 18 (4) (2011) 255–258.

[9] W. Hong, T.-S. Chen, H.-Y. Wu, An improved reversible data hiding in encrypted images using side match, IEEE Signal Process. Lett. 19 (4) (2012) 199–202.

[10] X. Zhang, Separable reversible data hiding in encrypted image, IEEE Trans. Inf. Forensics Secur. 7 (2) (2012) 826–832.

[11] W. Zhang, K. Ma, N. Yu, Reversibility improved data hiding in encrypted images, Signal Process. 94 (2014) 118–127.

[12] X. Wu, W. Sun, High-capacity reversible data hiding in encrypted images by prediction error, Signal Process. 104 (2014) 387–400.

[13] X. Ma, Z. Li, H. Tu, B. Zhang, A data hiding algorithm for H.264/AVC video streams without intra-frame distortion drift, IEEE Trans. Circuits Syst. Video Technol. 20 (10) (2010) 1320–1330.

[14] W. Huo, Y. Zhu, H. Chen, A controllable error-drift elimination scheme for watermarking algorithm in H.264/AVC stream, IEEE Signal Process. Lett. 18 (9) (2011) 535–538.

[15] S. Gujjunoori, B.B. Amberker, DCT based reversible data embedding for MPEG-4 video using HVS characteristics, J. Inf. Secur. Appl. 18 (4) (2013) 157–166.

[16] S. Bouchama, H. Aliane, L. Hamami, Reversible data hiding scheme for the H.264/AVC codec, in: Proceedings of International Conference on Information Science and Applications, 2013, pp. 1–4.

[17] S. Lian, Z. Liu, Z. Ren, H. Wang, Commutative encryption and watermarking in video compression, IEEE Trans. Circuits Syst. Video Technol. 17 (6) (2007) 774–778.

[18] S.-W. Park, S.-U. Shin, Combined scheme of encryption and watermarking in H.264/scalable video coding (SVC), in: New Directions in Intelligent Interactive Multimedia, vol. 142, 2008, pp. 351–361.

[19] D. Xu, R. Wang, Y.-Q. Shi, Data hiding in encrypted H.264/AVC video streams by codeword substitution, IEEE Trans. Inf. Forensics Secur. 9 (4) (2014) 596–606.

[20] D. Xu, R. Wang, Efficient reversible data hiding in encrypted H.264/AVC videos, J. Electron. Imaging 23 (5) (2014) 053022-1–053022-14.

[21] Z. Ni, Y.-Q. Shi, N. Ansari, W. Su, Reversible data hiding, IEEE Trans. Circuits Syst. Video Technol. 16 (3) (2006) 354–362.

[22] R.L. Rivest, J.C.N. Schuldt, Spritz–a spongy RC4-like stream cipher and hash function, Presented at Charles River Crypto Day, 2014, pp. 1–30.

[23] ITU-T Recommendation, Advanced Video Coding for Generic Audiovisual Services, ISO/IEC, 2012.

[24] Z. He, J. Cai, C.W. Chen, Joint source channel rate-distortion analysis for adaptive mode selection and rate control in wireless video coding, IEEE Trans. Circuits Syst. Video Technol. 12 (6) (2002) 511–523.

[25] YUV Video Sequences (Online), 2006. Available: ⟨http://trace.eas.asu.edu/yuv/

index.html〉.

[26] The H.264/AVC Joint Model (JM), ver. 10.2 (Online), 2006. Available: 〈http://iphome.hhi.de/suehring/tml/download/old_jm/〉.

[27] F. Bellifemine, A. Capellino, A. Chimienti, R. Picco, R. Ponti, Statistical analysis of the 2D DCT coefficients of the differential signal for images, Signal Process.: Image Commun. 4 (6) (1992) 477–488.

[28] M.J. Gormish, J.T. Gill, Computation-rate-distortion in transform coders for image compression, in: Proceedings of SPIE Image and Video Processing, 1993, pp. 146–152.

[29] Z. Wang, A.C. Bovik, H.R. Sheikh, E.P. Simoncelli, Image quality assessment from error visibility to structural similarity, IEEE Trans. Image Process. 13 (4) (2004) 600–612.

[30] Y. Liu, Z. Li, X. Ma, J. Liu, A robust data hiding algorithm for H.264/AVC video streams, J. Syst. Softw. 86 (8) (2013) 2174–2183.

[31] Y. Liu, M. Hu, X. Ma, H. Zhao, A new robust data hiding method for H.264/AVC without intra-frame distortion drift, Neurocomputing 151 (2015) 1076–1085.

[32] S. Lin, D.J. Costello, Error Control Coding: Fundamentals and Applications, Pearson-Prentice Hall, Upper Saddle River, New Jersey, 2004.